Baroclinicity Influences on Storm Divergence and Stratiform Rain: Subtropical Upper-Level Disturbances

LARRY J. HOPPER JR. AND COURTNEY SCHUMACHER

Department of Atmospheric Sciences, Texas A&M University, College Station, Texas

(Manuscript received 21 February 2008, in final form 22 August 2008)

ABSTRACT

Divergence structures associated with the spectrum of precipitating systems in the subtropics and midlatitudes are not well documented. A mesoscale model is used to quantify the relative importance different baroclinic environments have on divergence profiles for storms primarily caused by upper-level disturbances in southeastern Texas, a subtropical region. The divergence profiles simulated for a subset of the modeled storms are consistent with those calculated from an S-band Doppler radar. Realistic convective and stratiform divergence signals are also generated when applying a two-dimensional convective–stratiform separation algorithm to reflectivities derived from the mesoscale model, although the model appears to underestimate stratiform rain area. Divergence profiles from the modeled precipitating systems vary in magnitude and structure across the wide range of baroclinicities common in southeastern Texas. Barotropic storms more characteristic of the tropics generate the most elevated divergence (and thus diabatic heating) structures with the largest magnitudes. In addition, stratiform rain regions in barotropic storms contain thicker, more elevated midlevel convergence signatures than more baroclinic storms. As the degree of baroclinicity increases, stratiform area fractions generally increase while the levels of nondivergence (LNDs) decrease. However, some weakly baroclinic storms contain stratiform area fractions and/or divergence profiles with magnitudes and LNDs that are similar to barotropic storms, despite having lower tropopause heights and less deep convection. Additional convection forms after the passage of barotropic and weakly baroclinic storms that contain elevated divergence signatures, circumstantially suggesting that heating at upper levels may cause diabatic feedbacks that help to drive regions of persistent convection in the subtropics.

1. Introduction

Many studies have investigated how the vertical structure of divergence and diabatic heating associated with deep convection influences the large-scale dynamical response in the tropics, but the effect extratropical precipitating systems have on the large-scale circulation is not as well understood. Although individual mesoscale convective systems (MCSs) usually have lifetimes too short to significantly affect the environment at synoptic to planetary scales (>1000 km), Stensrud (1996) demonstrated that the cumulative effects of an entire group of MCSs in the southern Plains over three days caused significant changes in large-scale flow patterns. Model simulations including the diabatic effects of convection enhanced the baroclinicity and inflow of warm, moist low-level air and produced significant upper-level perturbations that encouraged additional convection to form. Global rainfall analyses and barotropic model runs performed over multiple years by Stensrud and Anderson (2001) showed that persistent MCS convection in central North America and Southeast Asia produces source regions for Rossby waves that alter midlatitude circulation patterns and encourage additional convection as well. One prominent example of this occurred during the 1993 Midwestern floods when a continuous succession of MCSs produced a 200-hPa divergence anomaly (Bell and Janowiak 1995) that Stensrud and Anderson (2001) collocated with tropical-like frequencies (>20%) of cloud-top temperatures $<-38°C$. Future research will have to determine if similar mechanisms caused persistent regions of deep convection responsible for widespread

Corresponding author address: Larry J. Hopper Jr., Dept. of Atmospheric Sciences, Texas A&M University, 3150 TAMU, College Station, TX 77843-3150.
E-mail: lhopper@ariel.met.tamu.edu

DOI: 10.1175/2008MWR2564.1

flooding in Texas, Oklahoma, and Kansas during the anomalous[1] spring and summer of 2007, during which some cases presented in this study occurred. This widespread, long-term flooding along with other significant shorter-term warm season flooding events in Texas since 1993 (e.g., southeast Texas in October 1994 and the Texas Hill Country in October 1998 and July 2002) underscore the importance of investigating the large-scale feedbacks of persistent midlatitude and subtropical deep convection.

In the tropics, the large-scale dynamical importance of separating rainfall into convective and stratiform components has been well established. Hartmann et al. (1984) forced a linear steady-state global model with Houze's (1982) idealized heating profiles and found that elevated heating structures associated with stratiform rain in MCSs produced a more realistic Walker circulation than a convective-only heating profile. DeMaria (1985) simulated a similar response to tropical heating from summertime convection in South America using an elevated heating profile. Schumacher et al. (2004) expanded upon these results by showing that horizontal variations in the latent heating profiles caused by geographical and temporal variations in stratiform rain estimated by the Tropical Rainfall Measuring Mission (TRMM) precipitation radar (PR) produced circulation anomalies of varying height and vertical extent. This large-scale response was even more sensitive to latent heating variations during El Niño when the east–west gradient in the stratiform rain fraction is more pronounced than usual, further highlighting the global circulation's sensitivity to variations in stratiform rain. However, the relative importance of stratiform rain in the large-scale circulation of the extratropics remains to be shown.

Tropical convection results from young, vigorous overturning cells, whereas stratiform rain results from older, less active convection (Houze 1997). In the subtropics and midlatitudes, stratiform rain also forms from large-scale lifting (i.e., a nonconvective source). Convective cells are generally ~1–10 km in horizontal dimension and contain strong maximum vertical velocities ($|w| \sim 1$–$50+$ m s^{-1}) and high rain rates (>5 mm h^{-1}). Stratiform rain covers larger areas (~100-km horizontal dimension) and has weaker vertical velocities ($|w| <$ 1 m s^{-1}) and lower rain rates (<5 mm h^{-1}; Houze 1993). Convective updrafts supply moisture to clouds and increase the time precipitation particles grow within them by collection until they fall out of updraft cores. Weaker, mesoscale updrafts above the 0°C level in stratiform rain regions enable precipitation particles to grow more slowly by vapor diffusion as they settle down from higher levels in the cloud, while evaporation occurs in mesoscale downdrafts below the 0°C level. As a result, vertical air motions associated with stratiform and convective rain induce two different atmospheric responses. Convective cells are characterized by strong convergence at low-levels and strong divergence aloft, whereas stratiform rain regions induce a three-layered response characterized by moderate convergence at the 0°C level and moderate divergence at lower and upper levels (Gamache and Houze 1982; Mapes and Houze 1993, 1995).

This study focuses on determining variations in divergence profiles associated with the convective and stratiform rain regions of subtropical upper-level disturbances with varying degrees of baroclinicity in southeast Texas. Horizontal divergence profiles are presented instead of diabatic heating because divergence is more directly observed. Mean divergence profiles simulated by a mesoscale model are compared to radar observations for validation. Once differences in divergence across varying degrees of baroclinicity are established, future work will focus on extending these results to the subtropics as a whole and developing idealized diabatic heating profiles to investigate their climatological impact on the global circulation.

2. Baroclinicity in the subtropics

Southeast Texas, a subtropical location, experiences a wide range of background environments commonly found in both the tropics and midlatitudes, making the region ideal for investigating how storm divergence and stratiform rain production varies with baroclinicity. Purely barotropic conditions—where pressure surfaces are vertically stacked, the direction and speed of geostrophic wind is independent of height, and no horizontal temperature gradients exist—are highly idealized and rarely exist simultaneously even in tropical environments. Equivalent barotropic atmospheres, where thickness and height contours are parallel in the presence of horizontal temperature gradients, are more common and dictate that the geostrophic wind speed may vary with height while maintaining constant direction (Wallace and Hobbs 1977). These equivalent barotropic environments are common in the subtropics during summer when the strength and southern penetration of midlatitude cyclones decrease, causing weak horizontal temperature gradients and vertical wind shears.

Fritsch and Forbes (2001) noted that convective systems forming in more barotropic environments depend more strongly on features and processes imposed by the convection itself, such as the moist-downdraft production

[1] According to the National Climatic Data Center (NCDC), June–August 2007 was Texas's wettest summer and Oklahoma's fourth wettest summer on record. Similarly, March 2007 was Texas's wettest March on record.

of a surface-based cold pool and the large stratiform cloud shield characteristic of mesoscale convective complexes. Conversely, when baroclinic conditions with strong horizontal temperature gradients and vertical wind shears common to the midlatitudes predominate, storms have a much less active large-scale feedback and develop primarily from externally imposed forcings like mesoscale components of synoptic-scale baroclinic systems. However, a mixture of barotropic and baroclinic conditions appear to occur during the transitional seasons of spring and autumn in southeast Texas, when most convective systems form in weakly baroclinic background environments with either moderate horizontal temperature gradients, wind shears, or a combination of both. Although additional research is needed to better quantify subtropical baroclinicities, subtropical locations such as southeast Texas frequently experience storms within weakly baroclinic environments that may have a greater convective feedback on the large-scale circulation than previously thought.

3. Methods

a. Model

Model simulations of each case were conducted using the fifth-generation Pennsylvania State University–National Center for Atmospheric Research (NCAR) Mesoscale Model, version 3.7 (MM5; Dudhia 1993). The 27-km-resolution outermost coarse domain (D1) consists of 133 × 133 grid points with 27 vertical sigma levels covering much of the continental United States and Mexico (Fig. 1). The second domain (D2) incorporates 130 × 130 grid points with 9-km grid spacing, while the innermost 3-km-resolution domain (D3) contains 100 × 100 grid points. Initial and lateral boundary conditions were created using the National Centers for Environmental Prediction (NCEP) global final tropospheric analysis with 1° horizontal and 6-h temporal resolution, and two-way nesting is utilized for the lateral boundary conditions of D2 and D3. Table 1 displays the initialization time of each model run presented in this study, along with the time periods over which the model-derived calculations are taken and over which the modeled storm best compares to Next Generation Weather Radar (NEXRAD) imagery.

A uniform set of schemes is used to parameterize physical processes for each storm. Radiative processes are handled using a scheme that accounts for longwave and shortwave interactions in clouds and the clear atmosphere (Dudhia 1989). The planetary boundary layer is parameterized with a high-resolution Blackadar (1976, 1979) scheme adapted for MM5 by Zhang and Anthes (1982) and Zhang and Fritsch (1986) that incorporates the effects of moist vertical diffusion in clouds. Although a cumulus scheme is not used for either of the nested domains (D2 and D3), the Grell (1993) cumulus parameterization is used on the coarse domain (D1). Finally, the Goddard explicit microphysics parameterization (Lin et al. 1983; Tao and Simpson 1993), which includes cloud ice, snow, and graupel processes, is used on each domain.

Model-derived horizontal divergence and radar reflectivity (hereafter referred to as MM5 reflectivity) are both calculated over D3 (excluding the outermost five grid squares) during the times for which convection occurred on D3 for each storm. Radar reflectivity calculations are based on Stoelinga's (2005) algorithm, which assumes the size distribution of hydrometeors follows an exponential distribution with fixed intercepts of 8×10^6, 2×10^7, and 4×10^4 m^{-4} for rain, snow, and graupel, respectively. Particles are also assumed to be spheres with constant densities of 1000, 100, and 400 kg m^{-3} for rain, snow, and graupel, respectively. The mean horizontal divergence profiles shown in sections 4 and 5 only include grid squares in a vertical column whose near-surface MM5 reflectivity exceeds 5 dBZ to provide a more direct comparison to past radar studies. MM5 reflectivity and horizontal divergence is also objectively classified as convective or stratiform using Steiner et al.'s (1995) radar-based algorithm.

b. Convective–stratiform separation algorithm

Convective and stratiform precipitation areas are identified using a radar technique based on the horizontal structure of the precipitation field (Steiner et al. 1995). In this study, the Steiner et al. (1995) separation algorithm is applied to MM5 reflectivities at the seventh half-sigma level above the surface (~1.6 km) that exceed 5 dBZ. Selecting a level lower than the 3 km Steiner and his colleagues originally used is necessary because midlatitude environments have more variable melting levels than in the tropics where the bright band is almost always found above 3 km. A lower separation level is also more practical in cooler and drier midlatitude environments because they tend to undergo more significant amounts of evaporation in the lower troposphere.

Convective centers are identified in the Steiner et al. (1995) separation algorithm for grid points whose reflectivities exceed a specified threshold or are significantly higher than nearby reflectivity values. Any grid point in the MM5 reflectivity field that exceeds 40 dBZ is classified as a convective center. Grid points that have reflectivities below 40 dBZ may still be classified as a convective center if the reflectivity at that point differs from the mean reflectivity (of all echoes greater than 5 dBZ) taken over the grid point's surrounding

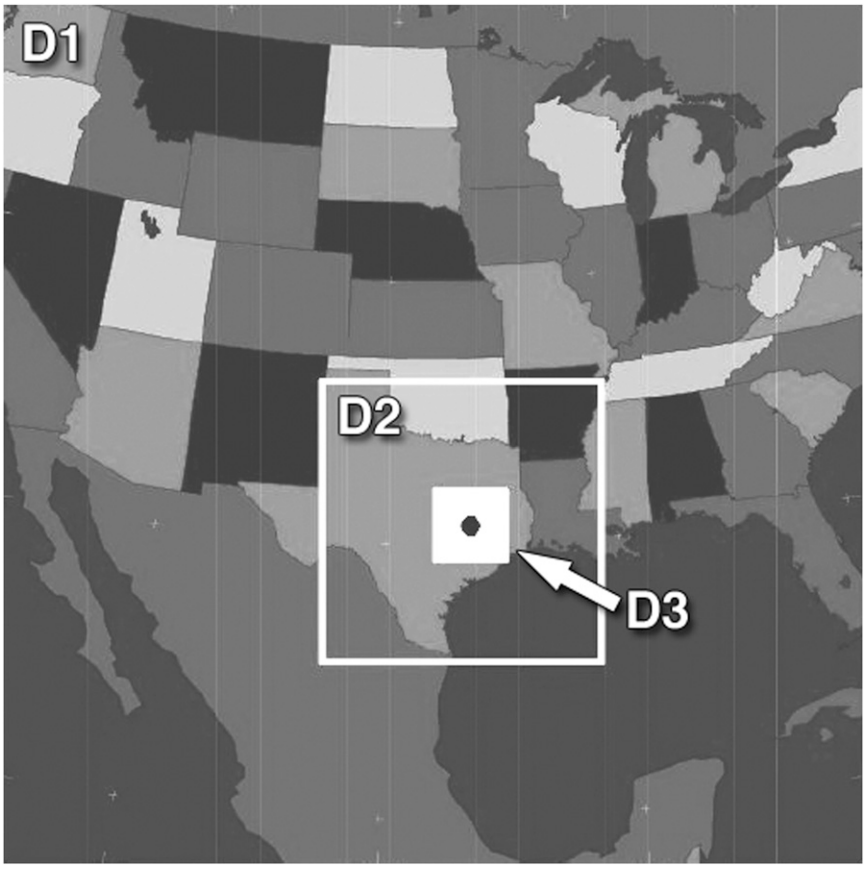

FIG. 1. The MM5 model domains. The grid resolutions of the outermost coarse domain 1 (D1), domain 2 (D2), and the innermost analysis domain 3 (D3) are 27, 9, and 3 km, respectively. ADRAD's position is indicated by the dot near the center of D3 (30.62°N, 96.34°W).

background radius of 11 km (Z_{bg}; dBZ) by at least the difference (ΔZ; decibels) given by a quadratic function in Steiner et al. (1995). This study uses a cosine form of the quadratic function [Eq. (1)], which is described in Yuter and Houze (1997) and makes adjusting the algorithm's parameters more intuitive.

$$\Delta Z = 10 \cos(\pi Z_{bg}/87.5), \quad 0 \le Z_{bg} < 43.75. \qquad (1)$$

This peakedness criteria curve has a shape similar to Steiner et al.'s (1995) quadratic function and contains very small changes in magnitude (<0.3 dB) to better satisfy model-derived convection that generally produces higher than observed reflectivities. Once convective centers are identified, a 1–5-km radius surrounding each core is also classified as convective using an intensity-dependent step function [this study uses the ''medium'' relation shown in Fig. 6b of Steiner et al. (1995)]. The remainder of the precipitation is classified as stratiform.

Sensitivity studies performed on the peakedness criteria indicate that changing this curve alters stratiform area fractions, but has little effect on the divergence profiles generated for stratiform and convective rain regions. Sensitivity studies performed for the surrounding area criterion yield smaller changes in divergence and stratiform area fractions than when tuning the portions of the algorithm that determine the convective centers themselves. In addition, the stratiform area calculations have little dependence on the area over which data are processed (D3 in this study) as long as the area's radius exceeds 100 km. These findings suggest that the convective and stratiform divergence profiles generated by MM5 are robust instead of being an artifact of how the separation algorithm is tuned. As a final note, although the convective–stratiform rain separation can be done using other model parameters (Lang et al. 2003), we have chosen to use a reflectivity-based approach in order to better compare our model results with radar observations and past radar studies.

c. *Radar observations and VAD divergence*

Observational results from the Texas A&M University S-band Aggie Doppler Radar (ADRAD) are used

TABLE 1. List of the storms in barotropic (BT), weakly baroclinic (WB), and strongly baroclinic (SB) environments modeled with their individual initialization times in MM5 along with the time periods over which the model calculations over the analysis domain (D3) are performed and the time periods these calculations are meant to represent as seen in NEXRAD observations.

Storm/model run (baroclinicity)	Initialization date and time	MM5 analysis time	NEXRAD analysis time
20 Jul 2007 (BT)	0000 UTC 20 Jul 2007	1500–2300 UTC 20 Jul	0900 UTC 20 Jul–0000 UTC 21 Jul
13–14 Mar 2007 (WB)	1200 UTC 13 Mar 2007	1700 UTC 13 Mar–1100 UTC 14 Mar	1700 UTC 13 Mar–1200 UTC 14 Mar
14–15 Mar 2007 (WB)	1200 UTC 13 Mar 2007	1400 UTC 14 Mar–0400 UTC 15 Mar	1200 UTC 14 Mar–0400 UTC 15 Mar
7–8 Apr 2007 (SB)	0000 UTC 7 Apr 2007	1100 UTC 7 Apr–1200 UTC 8 Apr	0900 UTC 7 Apr–1200 UTC 8 Apr
4 Jul 2006 (BT)	0000 UTC 4 Jul 2006	1000–2300 UTC 4 Jul	1100–2300 UTC 4 Jul
26–27 Mar 2007 (WB)	0000 UTC 26 Mar 2007	1900 UTC 26 Mar–1100 UTC 27 Mar	1800 UTC 26 Mar–0900 UTC 27 Mar
25 Feb 2006 (SB)	0000 UTC 25 Feb 2006	0500–2200 UTC 25 Feb	0400–2200 UTC 25 Feb

to show that the mean divergence profiles generated by MM5 for the cases presented in section 4 are reasonable and that the methodologies utilized in this study may be applied across varying storm types and baroclinicities. ADRAD is located in College Station, Texas (30.6°N, 96.3°W), near the center of the D3 model domain (Fig. 1). A volume scan strategy is run every 10 min and includes 16 elevation angles ranging from 0.5° to 33° (except for the 7 April 2007 storm, which only uses 12 elevation angles ranging from 0.5° to 14.3°).

Mean divergence profiles from ADRAD are generated using a code developed by Mapes and Lin (2005) for tropical convection that incorporates Browning and Wexler's (1968) velocity-azimuth display (VAD) technique. Instead of remapping the radar data to a Cartesian grid, the horizontal space of ADRAD's data is binned into polar coordinates temporally using a space–time binning algorithm (CYLBIN) to retain the range-dependent aspects of the radar's sampling characteristics and to better interpret radial velocities. Hourly data are separated into 500-m vertical layers and placed in a coarse horizontal grid with twenty-four 15° bins in azimuth and twelve 8-km bins in range. Histograms of unfolded mean radial velocities are retained for each spatial grid cell and are used to calculate mean horizontal divergence using the VAD technique.

Because data are generally sparse at upper levels, the Mapes and Lin (2005) code repools all data from 500-m height layers into 50-hPa pressure layers so that some pressure levels farther aloft will have multiple measurements available for analysis. Additionally, VAD divergence estimates from ADRAD pool data in the horizontal by supplementing the data in each 8-km range interval with data from both adjacent 8-km annuli. The five-range pooled observed divergence profiles presented in section 4 include the most data with four sets of 40-km annuli centered about 28, 44, 60, and 76 km from ADRAD's center. Similarly, the three-range pooled and raw divergence profiles include four sets of 24- and 8-km annuli, respectively, centered about the same radii as the five-range pooled data. Although pooling the data in range and height introduces small sources of error, the cases investigated in this study and those shown by Mapes and Lin (2005) indicate that the benefits of increasing data coverage in azimuth and at upper levels to improve mean divergence estimates far outweigh the potential drawbacks. Likewise, the mean divergence estimates using range pooled data from ADRAD are in better agreement with the model-derived mean divergence calculations than those without range pooled data.

4. Model and observational comparisons by baroclinicity

In this section, three storms associated with upper-level disturbances but with disparate degrees of baroclinicity are modeled. A similar synoptic forcing was chosen to isolate the effect of baroclinicity on storm divergence profiles. Investigating upper-level disturbances is critical to understanding how storm divergence varies in the subtropics because they are the only synoptic forcing that is prevalent across a wide range of baroclinic environments (including barotropic). In addition, this section compares the model-derived mean divergence profiles with ADRAD's. Supplementary upper-level disturbances are modeled in section 5 to show that the results presented in this section are robust. Table 1 lists the storms investigated in this section and section 5.

a. Barotropic case: 20 July 2007

Scattered convection formed in a barotropic environment on 20 July 2007 during a period of persistent

convection in Texas that began almost a week earlier. Thunderstorms developed along a tropical shortwave evident at 700–500 hPa near the upper Texas Gulf coast around 0900 UTC and rapidly increased in areal coverage by forming large stratiform regions as the system propagated inland later that morning and afternoon. Although MM5 simulates the evolution of convection reasonably well, convection does not develop until 1500 UTC. This time discrepancy may occur because the model was initialized too late (0000 UTC) to accurately simulate diabatic feedbacks from the previous day's convection. However, model runs initialized on 1200 UTC 19 July at do not produce convection at the appropriate time either. Figures 2a,b display a snapshot comparison of the radar reflectivities determined by NEXRAD and MM5, respectively, for this storm. The NEXRAD and model-derived radar images shown throughout this study correspond to similar points in the storm's evolution as opposed to an actual time matchup. The NEXRAD images shown in Figs. 2, 7, and 11 were obtained from the Mesoscale and Microscale Meteorology Division of NCAR's Internet image archive (available online at http://www.mmm.ucar.edu/imagearchive/).

The synoptic flow pattern over the central United States was dominated by a strong ridge of high pressure that stretched as far north as southern Manitoba and Saskatchewan. Aside from some weak boundary-layer shear and some semblance of a weak shortwave, the environment was essentially barotropic on 20 July. Convection formed the following two days before a weak cold front moved in, providing the region with a reprieve from rain on 23–24 July before convection began again on 25 July. This storm is representative of many of the rain events that occurred in Texas during the summer of 2007 when convection did indeed seem to be ''gregarious'' and ''persistent'' in the sense Mapes (1993) generalized for tropical convection and Stensrud and Anderson (2001) described for the 1993 Midwestern floods, respectively.

Figure 3a shows that the model-derived mean divergence profile is characterized by convergence at low- and midlevels and divergence aloft. Divergence is also present near the surface because of convective outflow. All of these features are present in the calculated divergence from ADRAD (Fig. 3b). As expected, the five- and three-range pooled radar data produce smoother divergence profiles in closer agreement with each other and the model than the divergence profile using data from just one 8-km annuli. Hereafter, only the five-range pooled profiles are plotted. The model-derived level of nondivergence (LND) at 6.8 km is also very close to the 7.0-km LND observed by ADRAD (Table 2), suggesting that MM5 is accurately simulating the depth of convection.

In addition, robust stratiform and convective divergence signals (Fig. 3a) are produced when Steiner et al.'s (1995) separation algorithm is applied to MM5 reflectivities. The stratiform profile contains moderate midlevel convergence peaking at the 0°C level near 5 km, along with moderate upper- and lower-level divergence. The convective profile has strong convergence at lower levels with a maximum just above 1 km and strong divergence at upper levels. Similar to previous studies, the stratiform LND is 3.4 km higher than the convective LND (Table 2). The maximum magnitudes of convergence and divergence in MM5 are approximately 4 times greater in convective regions than they are in stratiform regions in agreement with Gamache and Houze's (1982) sounding-based calculations of a tropical squall line. MM5′s mean divergence magnitudes are a factor of 2 larger than ADRAD's, but they are less than or similar to many of the hourly divergence profiles presented in Mapes and Lin (2005) and other tropical Doppler-based studies (e.g., Mapes and Houze 1995). Although MM5 may be overpredicting divergence magnitudes, this disagreement may also be caused by the different methods used to calculate divergence, particularly at upper levels where ADRAD's data are sparse and thus more uncertain.

Although the stratiform LND's placement is close to that found by Gamache and Houze (1982) and other tropical case studies, the convective LND is 1.5–2 km higher in MM5. One reason for this elevated convective LND might be that the separation algorithm is misclassifying stratiform rain as convective. The stratiform area fraction generated by the Steiner et al. (1995) algorithm for this storm is 58.3% (Table 2), considerably less than the tropicswide mean of 73% Schumacher and Houze (2003) found using TRMM PR data. However, increasing the stratiform area fraction to 63% by liberally altering the algorithm does not change the convective profile's LND and only causes small increases in its peak magnitudes. Therefore, the modeled storm may have deeper low-level convergence in the convective region than a typical tropical case, or MM5 may be misrepresenting deep convective mass transport. MM5 is still probably underpredicting the stratiform rain area for this storm, which could in part account for the slightly lower model-derived mean LND compared to the observed LND calculated from ADRAD.

Histograms of the MM5 reflectivities within stratiform and convective regions capture some of the major microphysical differences between these two rain types, but also indicate some flaws. Figures 4a,b display the vertical distribution of reflectivity within stratiform and convective regions, respectively, using a frequency by

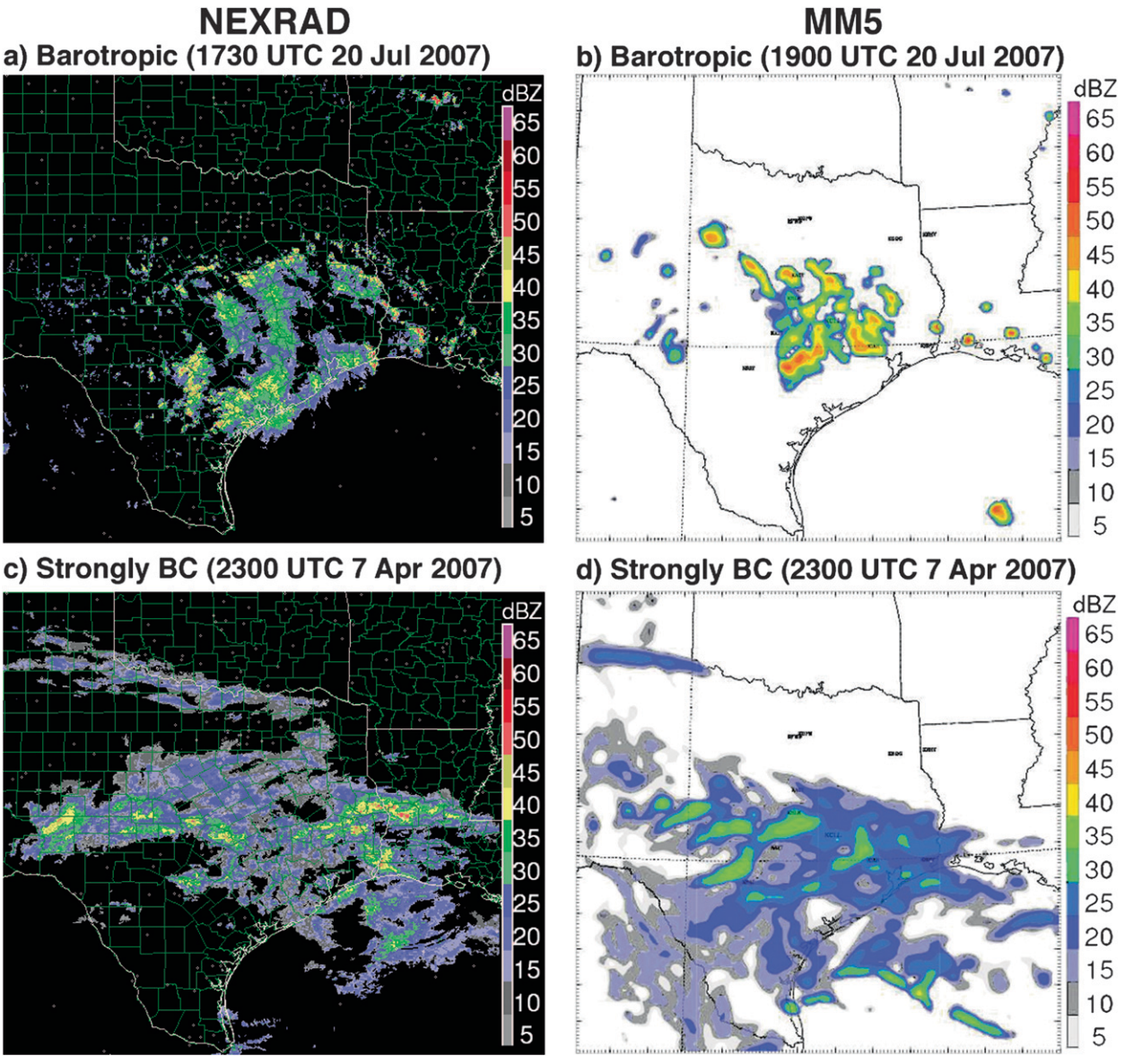

FIG. 2. (a) NEXRAD and (b) MM5 reflectivity over D2 at the times indicated for the barotropic case presented in section 4a. (c) NEXRAD and (d) MM5 reflectivity over D2 at the times indicated for the strongly baroclinic case presented in section 4b.

altitude diagram that will be used throughout this study. Each line represents a 10% quantile (from 10% to 90%) of echo occurrence with height. The plots are cut off at levels that do not have an adequate number of reflectivity values (<0.5% of the total count).

The stratiform MM5 reflectivities (Fig. 4a) exhibit a bright band at the 0°C level (4–5 km) and have a narrower distribution above this level than in the convective region where vertical velocities vary more. Although MM5 indicates that some graupel is present in the stratiform region, the mean snow mixing ratio is larger by a factor of 3 (not shown), implying diffusion is the dominant ice growth process. The stratiform reflectivity histogram is similar to those shown by Schumacher and Houze (2006) for the tropical east Atlantic and West Africa, but the near-surface median MM5 reflectivity of 22.75 dBZ is 2–3 dBZ lower, implying evaporative processes may be stronger for stratiform rain in this simulation. Reflectivities above the 0°C level in Fig. 4a also do not decrease with height as quickly as they do in Schumacher and Houze (2006), indicating that MM5 may overpredict snow and graupel aloft in stratiform regions. These deficiencies also occur when using the Reisner-2 microphysics scheme (Reisner et al. 1998).

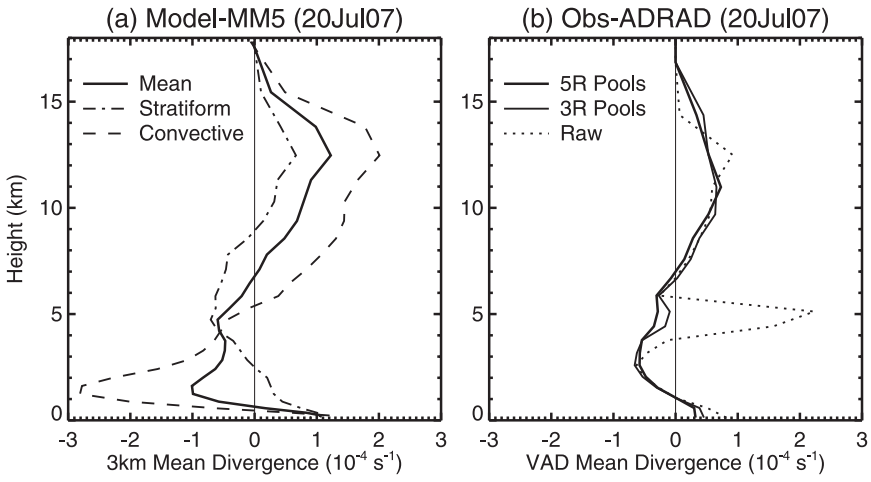

FIG. 3. (a) MM5-derived mean grid-scale divergence profiles based on half-hourly model data (solid) and divergence profiles for stratiform (dash–dot) and convective (dashed) rain types as defined by the Steiner et al. (1995) separation algorithm applied to MM5-derived radar reflectivities between 1500 and 2300 UTC 20 Jul 2007. The profiles include all grid boxes in a vertical column for which the surface radar reflectivity exceeds 5 dB*Z*. (b) Observed VAD (Mapes and Lin 2005) divergence profiles using ADRAD for five-range pooled data in 40-km annuli (solid), three-range pooled data in 24-km annuli (large dash with three smaller dashes), and the raw divergence from data in 8-km annuli (dotted). Each mean includes four sets of annuli centered about 28, 44, 60, and 76 km from ADRAD's center averaged hourly from 1500 to 1800 UTC. The mean divergence profile for the five-range pooled data is most closely analogous to the mean divergence in (a).

A broader reflectivity distribution above the 0°C level is visible in the convective regions (Fig. 4b) where riming plays a stronger role than diffusion for ice growth in this storm. Mean values of convective graupel mixing ratios in MM5 (not shown) peak near 6 km and are greater than those for snow at all levels, whose 8.5 km maximum is over a factor of two smaller. Convective reflectivities are 15–20 dB*Z* greater than their stratiform counterparts and have a near-surface median value of 40.75 dB*Z*, which is 3–4 dB*Z* higher than West African convection shown by Schumacher and Houze (2006). The convective reflectivity histogram also displays a bright band, albeit less pronounced than for the stratiform region, suggesting that the Goddard scheme may be biased toward stratiform microphysical processes. Nevertheless, the Goddard scheme is used for all cases in this study because it typically produces higher stratiform area fractions and more realistic reflectivity and divergence structures than Reisner-2.

Despite potential microphysical problems with the separated radar reflectivities, the algorithm appears to work from a kinematic perspective because it generates reasonable vertical velocity structures for stratiform and convective regions. As expected, the stratiform region

TABLE 2. List of the stratiform area fractions and the stratiform, convective, and mean levels of nondivergence (LNDs; km) generated by MM5 for the barotropic (BT), weakly baroclinic (WB), and strongly baroclinic (SB) storms modeled over the analysis time periods given in Table 1. The mean LND generated by ADRAD is also given for the storms presented in section 4.

Storm/model run (baroclinicity)	Stratiform area (%)	Stratiform LND (km)	Convective LND (km)	Mean LND (km)	ADRAD LND (km)
20 Jul 2007 (BT)	58.3	8.9	5.5	6.8	7.0
13–14 Mar 2007 (WB)	60.2	8.1	5.9	6.4	6.6
14–15 Mar 2007 (WB)	54.8	7.3	4.5	4.7	5.0
7–8 Apr 2007 (SB)	99.2	4.1	5.9	4.2	3.5
4 Jul 2006 (BT)	61.3	9.7	6.7	8.1	—
26–27 Mar 2007 (WB)	76.1	6.2	5.2	5.5	—
25 Feb 2006 (SB)	82.6	4.8	3.7	4.5	—

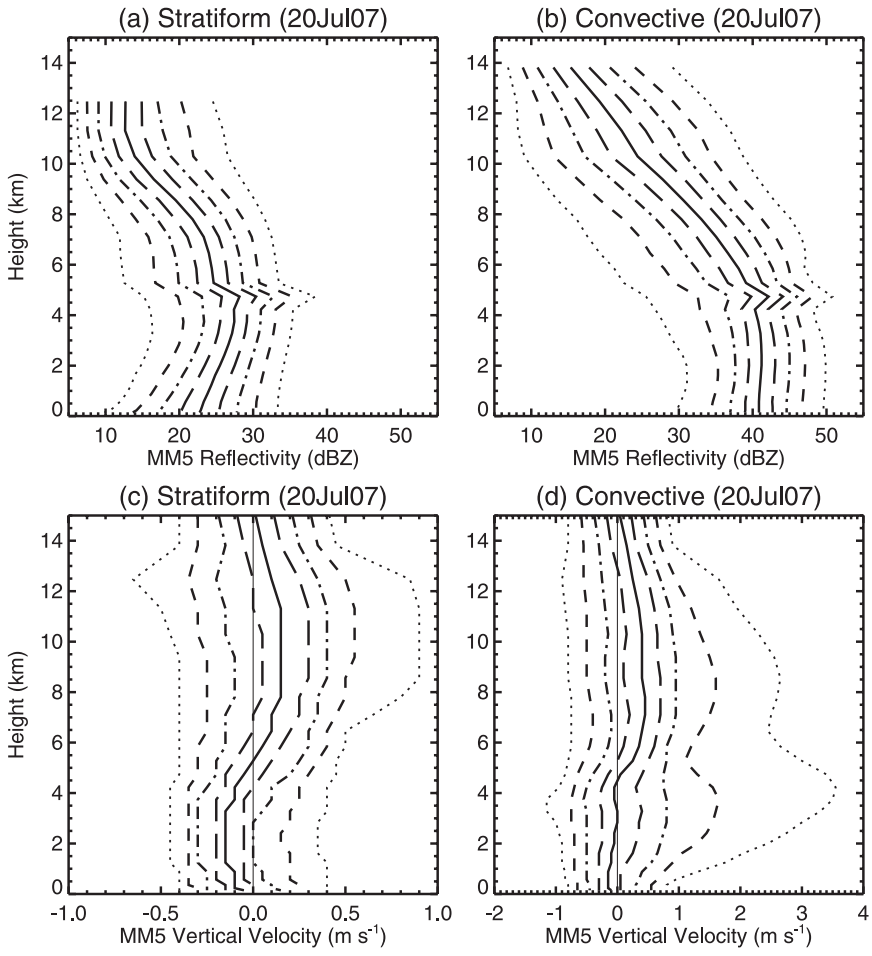

FIG. 4. Vertical distributions of (a),(b) radar reflectivity and (c),(d) vertical velocity for stratiform and convective rain types as defined by the Steiner et al. (1995) separation algorithm applied to MM5 reflectivities between 1500 and 2300 UTC 20 Jul 2007. The MM5 reflectivity profiles include all grid boxes in a vertical column for which the surface radar reflectivity exceeds 5 dB*Z*. Height levels with less than 0.5% of the total count are not plotted in the radar reflectivity plots. Each line represents a 10% quantile from 10% to 90%; the median profile is the solid, thick line.

(Fig. 4c) contains weak model-derived vertical velocities with magnitudes within ± 1 m s^{-1}, dominated by updrafts above 5 km (with ~20% of velocities from 8 to 12 km exceeding 0.5 m s^{-1}) and by less intense downdrafts below the melting level. The convective region (Fig. 4d) has more variation in vertical velocity with height, with 20%–40% of the velocities exceeding ± 1 m s^{-1} depending on the level evaluated. Downdrafts at the 10th percentile and updrafts at the 80th and 90th percentiles exhibit lower- and upper-level peaks as well (3.5 km for the downdrafts and 4 and 8.5 km for the updrafts). Cifelli and Rutledge (1998) found a prominent peak in diabatic heating near 4 km for tropical convection near Darwin, which suggests that MM5 may be accurately simulating deep convection. These realistic kinematic structures, along with the agreement between the model-derived divergence profiles with those calculated from ADRAD and from other tropical studies, suggest that MM5 may be used to study divergence of extratropical barotropic storms.

b. Strongly baroclinic case: 7–8 April 2007

During late fall, winter, and early spring, southeast Texas experiences stronger horizontal temperature gradients and vertical wind shears at the opposite end of the baroclinicity spectrum from the barotropic environment discussed in section 4a. This strongly baroclinic case study is primarily a stratiform storm system with a few embedded elements of elevated convection that occurred on 7–8 April 2007 (Figs. 2c,d). MM5 generally

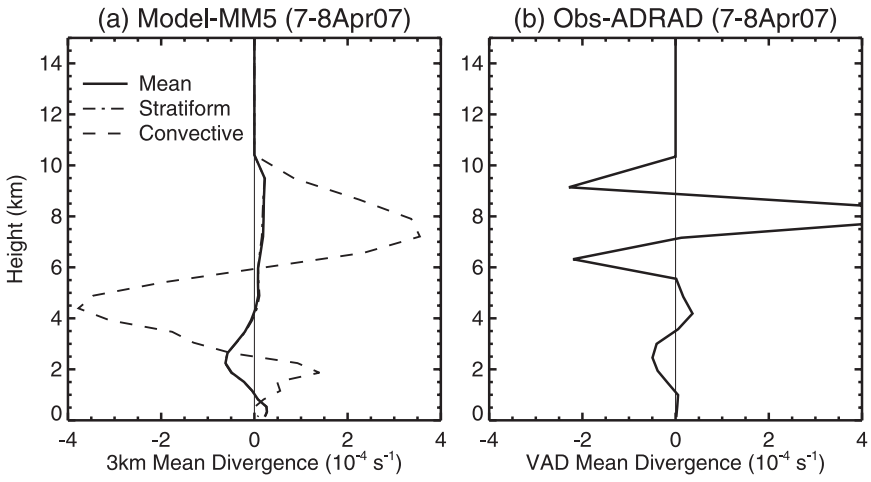

FIG. 5. (a) MM5-derived mean grid-scale divergence profiles for half-hourly data from 1100 UTC 7 Apr to 1200 UTC 8 Apr 2007. (b) Observed VAD divergence profiles for hourly averaged ADRAD data from 1900 UTC 7 Apr to 0000 UTC 8 Apr. The same plotting conventions are followed as in Fig. 3 except that only the five-range pooled data are plotted in (b).

matched the timing and placement of precipitation with observations throughout the storm's duration. An upper-level low in New Mexico, a developing subtropical jet, and a stationary front stretching from New Mexico into the Rio Grande Valley provided a focus for precipitation to develop around 0000 UTC 7 April. A cold front associated with a trough in the northeast United States and cloud cover north and west of D3 that inhibited daytime warming on 6 April caused a strong temperature gradient at low levels. This complex synoptic environment was devoid of any surface-based instability, but area soundings displayed elevated instability above a temperature inversion from 850 to 650 hPa with strong vertical shear and veering winds with height. As the storm evolved on 7 April, rain-induced evaporative cooling caused low-level temperatures to continue decreasing in southeast Texas, allowing wet snow and sleet to fall in parts of the northern half of D3. According to a public information statement issued by the National Weather Service office in League City, Texas, on 9 April 2007, this is the first time that accumulating snow has been recorded in southeast Texas during April.

Figure 5 shows that the model-derived mean divergence profile for this case is similar to ADRAD's and is in stark contrast to the barotropic case's mean divergence profile (cf. Fig. 3). The MM5 mean and stratiform divergence profiles (Fig. 5a) are almost identical in that they both contain convergence from 1.1 to 4.1 or 4.2 km with weak divergence below and above, similar to the divergence observed by ADRAD (Fig. 5b). ADRAD's data are too sparse to be utilized for comparison above 5.5 km, although some radar echoes above this level may be representative of the convective region. Table 2 shows that only 0.8% of the near-surface MM5 reflectivities were classified as convective and that the convective LND is 1.8 km higher than the stratiform LND, implying that convection in this case is more elevated than surface-based and that stratiform rain does not form from deep, surface-based convection. The model-derived convective divergence profile has larger magnitudes than the barotropic case (cf. Fig. 3a) as well, suggesting that the higher degree of baroclinicity may cause larger divergence magnitudes in convective regions. On the other hand, the model-derived stratiform convergence peak is of the same magnitude as that in the barotropic case ($\sim 7 \times 10^{-5}$ s^{-1}), albeit at a lower level (2–3 km).

Reflectivity structures for this storm are also much different than in the barotropic case. The stratiform reflectivity distribution (Fig. 6a) displays a median near-surface value of 25 dBZ and a trimodal structure with height, with reflectivity maxima at 5.5 km, 2 km, and the surface. The upper peak (which also occurs for the Reisner-2 scheme) is difficult to explain physically, but it may result from a small amount of convective rain being misclassified as stratiform and/or snow being overpredicted aloft. The lower two peaks are caused by phase changes associated with the strong temperature inversion aloft simulated in MM5 and observed in multiple area soundings released on 7–8 April that caused hydrometeors to melt from 2.5 to 4 km before attempting to refreeze from 0.5 to 2.5 km in the

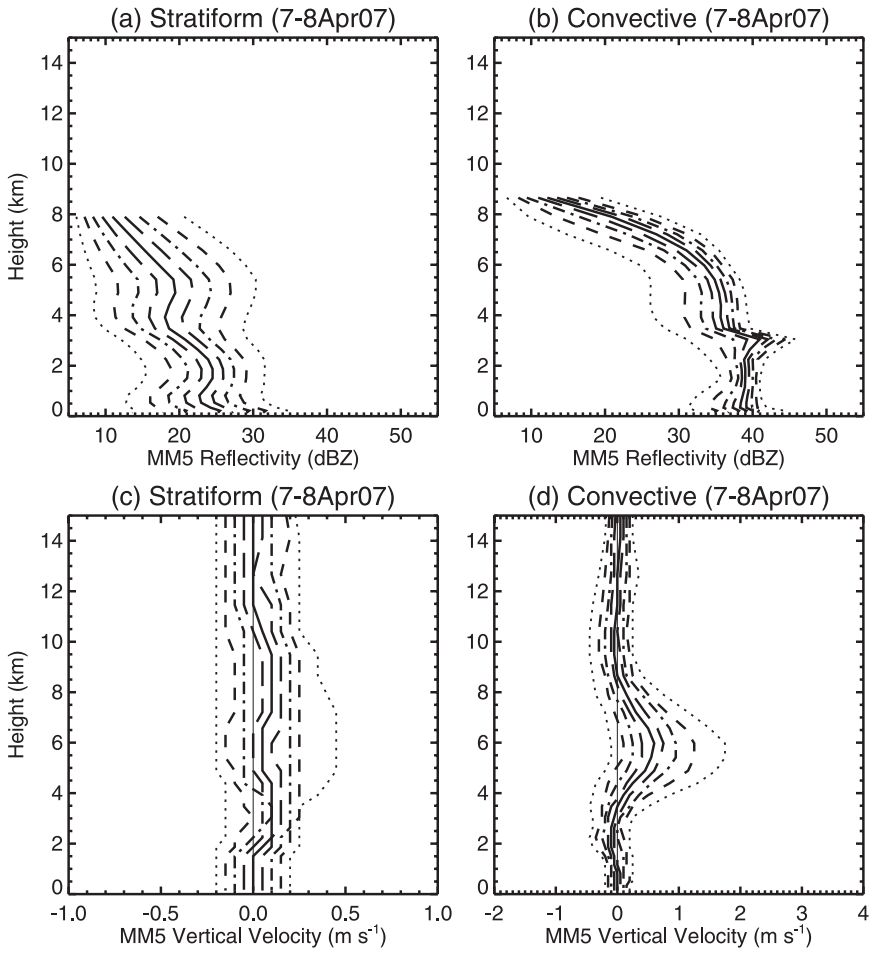

FIG. 6. Vertical distributions of (a),(b) radar reflectivity and (c),(d) vertical velocity for stratiform and convective rain in MM5 from 1100 UTC 7 Apr 2007 to 1200 UTC 8 Apr 2007 following the plotting convention in Fig. 5.

northern half to two-thirds of D3. Mixing ratios simulated by MM5 (not shown) indicate that rain is the dominant hydrometeor species between 1 and 2 km, below which snow and graupel mixing ratios are greater. This result is consistent with observations reporting sleet and snow at the surface. Snow is the dominant hydrometeor species above 2 km, with mean mixing ratios peaking near 5.5 km.

The convective reflectivity distribution (Fig. 6b) displays a higher median near-surface reflectivity of 39 dBZ, with over half of the isolated convective cores exhibiting a bright band near 3 km coinciding with a peak in the mean mixing ratio for graupel (not shown). However, above 3 km the mean mixing ratio for snow is considerably higher, peaking near 5.5 km at values 3 times greater than those for graupel. Therefore, diffusion is also the more prominent ice growth mechanism in the convective region, causing a much narrower reflectivity distribution aloft than occurs in the barotropic case where convective vertical velocities vary more and riming is more important.

Vertical velocities in the stratiform region (Fig. 6c) contain smaller magnitudes than in the barotropic case (cf. Fig. 4c) by about a factor of 2, with at least 60%–80% of the velocities having magnitudes below 0.2 m s^{-1} at every level. Some evidence of a weak updraft is present in the form of a velocity peak near 6 km, although it is considerably lower than in the barotropic case. Updraft velocities at midlevels are much more pronounced within the convective region (Fig. 6d), where over 20% of the vertical velocities exceed 1 m s^{-1} in a very narrow layer from 4.5 to 6.8 km. Over 80% of the convective vertical velocities below 3 km fall between -0.5 and $+0.3$ m s^{-1}, further differentiating the more elevated nature of convection in this strongly baroclinic storm from the less baroclinic cases presented

in this study that have much broader convective vertical velocity distributions in the lower troposphere. Despite applying Steiner et al.'s (1995) observational technique to MM5 reflectivities at a level (~1.6 km) where convective and stratiform vertical velocities are similar, the algorithm captures the kinematic differences that distinguish stratiform from convective regions well even though their vertical velocities only differ at midlevels. Therefore, Steiner et al.'s (1995) algorithm, which was originally developed for tropical radar data, may have potential for classifying MM5 reflectivities in strongly baroclinic storms with elevated convection that is more common in the midlatitudes.

c. *Weakly baroclinic cases: 13–14 and 14–15 March 2007*

Southeast Texas regularly experiences barotropic conditions in summer and strongly baroclinic storms from the midlatitudes in winter, early spring, and late autumn. However, many of the precipitating systems the region commonly experiences during spring and autumn, and during more anomalous periods in summer and winter are weakly baroclinic. These storms have significantly weaker temperature gradients and wind shears than typically found in stronger winter storms, but have too much synoptic forcing to be classified as barotropic.

Two weakly baroclinic MCSs occurred in succession on 13–15 March 2007 as a closed low pressure system stretching through the depth of the troposphere slowly moved east across Texas. This low pressure system originated from an intensifying lee trough on 10–11 March before becoming cutoff in west Texas and retrograding into southeast New Mexico on 12 March. A kicker shortwave weakened a ridge of high pressure off the California coast and eventually caused the low pressure system to begin a slow eastward progression across Texas late on 13 March. These complex dynamic elements created an environment with moderate speed and directional vertical wind shears that fall between those in the barotropic and strongly baroclinic cases. Area soundings also displayed a moderate amount of instability above a capped boundary layer. A weak temperature gradient was present because temperatures were unable to rebound quickly in parts of west Texas from a cold front that passed through on 11–12 March.

Convection began around 1500 UTC 13 March along a line in south Texas extending from Corpus Christi to Laredo. The line quickly moved northeast and increased in areal coverage throughout the afternoon to form a large, disorganized MCS with numerous pockets of intense convective cores. By 2300 UTC, the convection began to align itself in a series of small lines on the southern and eastern sides of the MCS where an outflow boundary left behind by the original convection was initiating new convective cells and reinforcing existing ones (Fig. 7a). The MM5 model run for this storm is delayed by about 3 h but simulates the system fairly well by placing most convection on the southern and eastern sides of the MCS with convective pockets embedded within stratiform rain elsewhere, although it fails to develop convection in northeast Texas outside D3 (Fig. 7b). The same model run extended farther in time is used to simulate the additional convection that began to develop the next morning around 1400 UTC 14 March in two places: in central Texas in the vicinity of the closed low pressure system aloft and along the same coastal outflow boundary responsible for enhancing convection the previous evening (now centered near Matagorda Bay). By 2000 UTC, the convection in central Texas increased in size and developed a small mesoscale convective vortex coinciding with the closed low pressure system as it propagated southeast during the afternoon and evening hours. MM5 initiates the convection in central Texas that accounts for almost all of the convection that occurs in D3, simulating a smaller MCS with a greater proportion of convective rain than occurred on the previous day. As a result, the 13–14 March storm has a higher stratiform area fraction (60.2%) than on the following day (54.8%; Table 2).

As in the previous case studies, MM5 generates realistic mean divergence profiles that are comparable to those observed by ADRAD. The structures of the model-derived divergence for both 13–14 March (Fig. 8a) and 14–15 March 2007 (Fig. 8c) exhibit convergence at low-to-midlevels sandwiched between near-surface and upper-level divergence, in close agreement with the observed divergence profiles shown in Figs. 8b and 8d, respectively. The model-derived mean LNDs for both cases are only 0.2–0.3 km below those observed by ADRAD, although the the 13–14 March storm's mean LND is 1.7 km higher (Table 2). The convective and stratiform LNDs are also more elevated in the 13–14 March case, which has a thicker layer of stratiform convergence from 1.6 to 8.1 km as compared with the following day's storm whose layer only extends from 3.0 to 7.3 km. MM5 reflectivity histograms shown in Fig. 9 indicate that convection extends up to heights that are 2 km higher on 13–14 March than on the following day when the LND is lower. Soundings from Fort Worth, Texas, show a 1-km decrease in the tropopause height from 0000 UTC 14 March to 0000 UTC 15 March associated with the increased baroclinicity from the passage of the upper-level low. This lowered tropopause caused a less-elevated divergence profile on 14–15 March because it prevented convective cells from

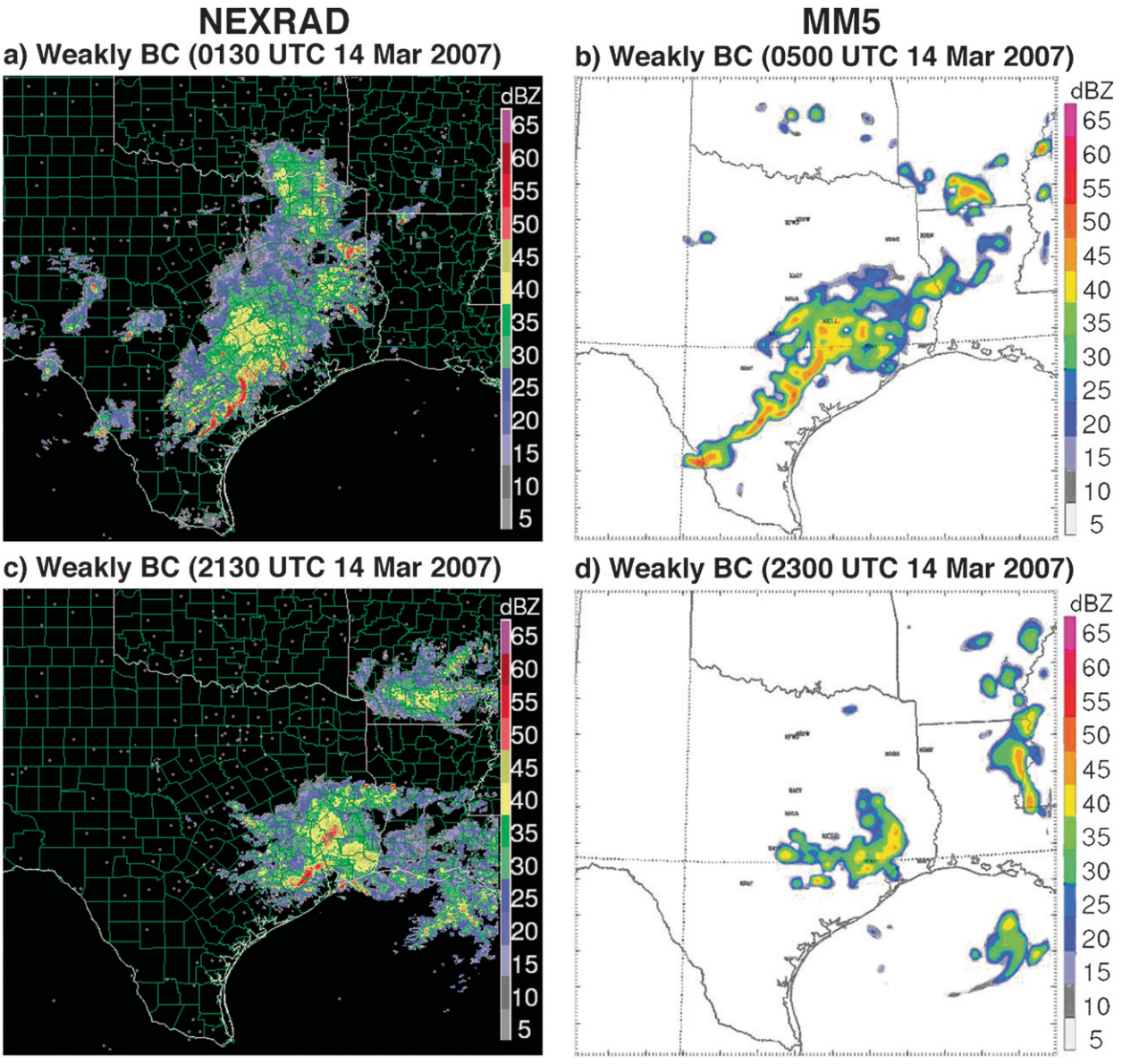

FIG. 7. (a),(c) NEXRAD and (b),(d) MM5 reflectivity over D2 at the times indicated for the weakly baroclinic cases presented in section 4c.

reaching as high as on 13–14 March. Nevertheless, both weakly baroclinic storms have much higher LNDs and upper-level divergence maxima than the strongly baroclinic case (cf. Figs. 5a,b) that occurred over 3 weeks later when, climatologically, the equilibrium level is higher and the degree of baroclinicity is lower. This suggests that interseasonal variabilities in these parameters are not negligible.

In agreement with the barotropic and strongly baroclinic cases, the model-derived divergence magnitudes on 13–14 March (Fig. 8a) are greater than those observed by ADRAD (Fig. 8b), which contains smaller magnitudes than observed on 14–15 March (Fig. 8d). However, unlike the cases presented previously, the observed divergence magnitudes on 14–15 March are actually greater than those derived in MM5 (Fig. 8c). These differences are caused at least in part by ADRAD oversampling stratiform regions on 13–14 March and convective regions on 14–15 March relative to the rest of southeast Texas. This occurred because most of the convection on 13–14 March was south of ADRAD's analysis range (but was still captured within MM5's analysis domain, or D3), whereas most of the convection that developed on 14–15 March formed within

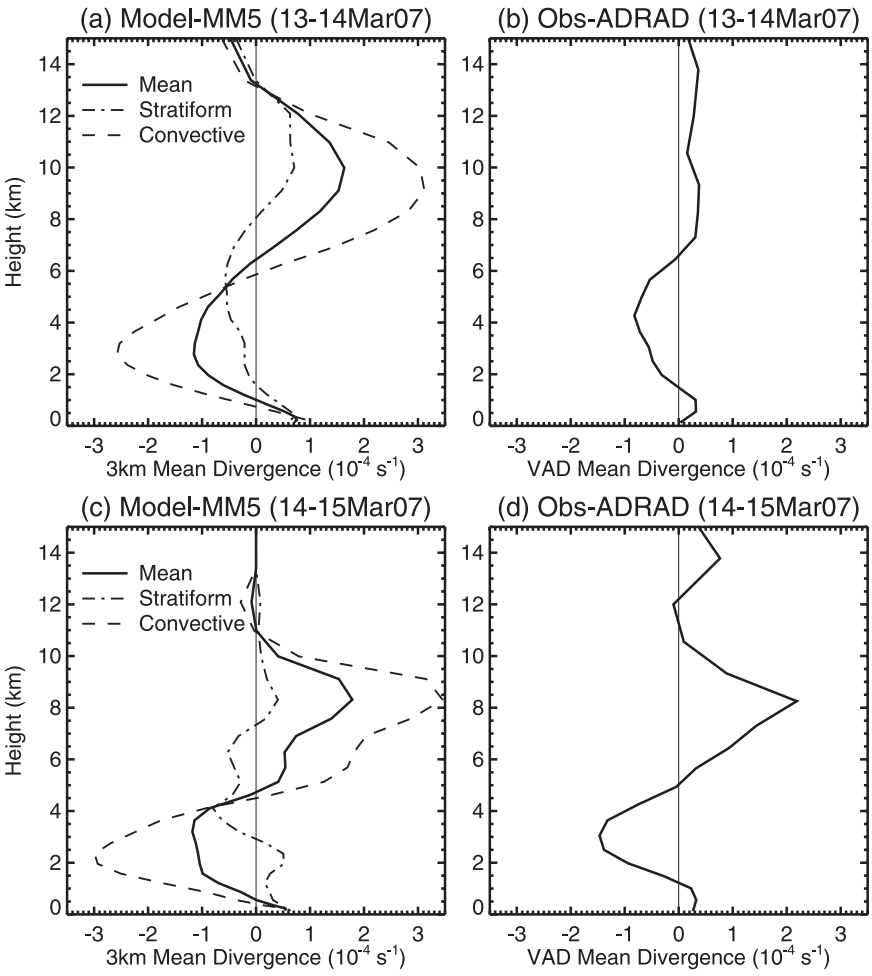

FIG. 8. (a) MM5-derived mean grid-scale divergence profiles for half-hourly data from 1700 UTC 13 Mar to 1100 UTC 14 Mar 2007. (b) Observed VAD divergence profile for hourly averaged ADRAD data from 1900 UTC 13 Mar to 0500 UTC on 14 Mar. (c) MM5-derived mean grid-scale divergence profiles for half-hourly data from 1400 UTC 14 Mar to 0400 UTC 15 Mar 2007. (d) Observed VAD divergence profile for hourly averaged ADRAD data from 1800 to 2300 UTC 14 Mar. The same plotting conventions are followed as in Fig. 3 except that only the five-range pooled data are plotted in (b) and (d).

ADRAD's analysis range, likely causing stratiform rain regions to be undersampled.

Radar reflectivity and vertical velocity histograms for both weakly baroclinic storms are presented for consistency. MM5 reflectivities within the stratiform region on 13–14 March (Fig. 9a) are ~4 dBZ higher than on 14–15 March (Fig. 9c), while the convective reflectivities (Figs. 9b and 9d) are only ~1 dBZ greater. The stratiform vertical velocity distribution on 13–14 March (Fig. 10a) exhibits a prominent updraft that peaks near 8.5 km and a slightly weaker downdraft that peaks near 3.5 km. Stratiform vertical velocities are weaker and less pronounced on 14–15 March (Fig. 10c), particularly at upper levels. This is consistent with decreases in the mean snow mixing ratio (not shown) and stratiform reflectivities on 14–15 March, indicating that mesoscale growth processes at upper levels are less enhanced than on 13–14 March. The larger, more elevated convective vertical velocities on 13–14 March (Fig. 10b) compared to the following day (Fig. 10d) implies that larger values of diabatic heating extend through a greater vertical extent of the troposphere on 13–14 March. Although the barotropic case has larger vertical velocities above 8 km within the convective region (cf. Fig. 4d), the 13–14 March case has larger magnitudes elsewhere with a higher peak in convective updrafts near 5.5 km. Therefore, although lower tropopause heights in the weakly baroclinic cases prevent convection from reaching as high as in the barotropic case, magnitudes of convective updrafts and downdrafts in the 13–14 March storm are

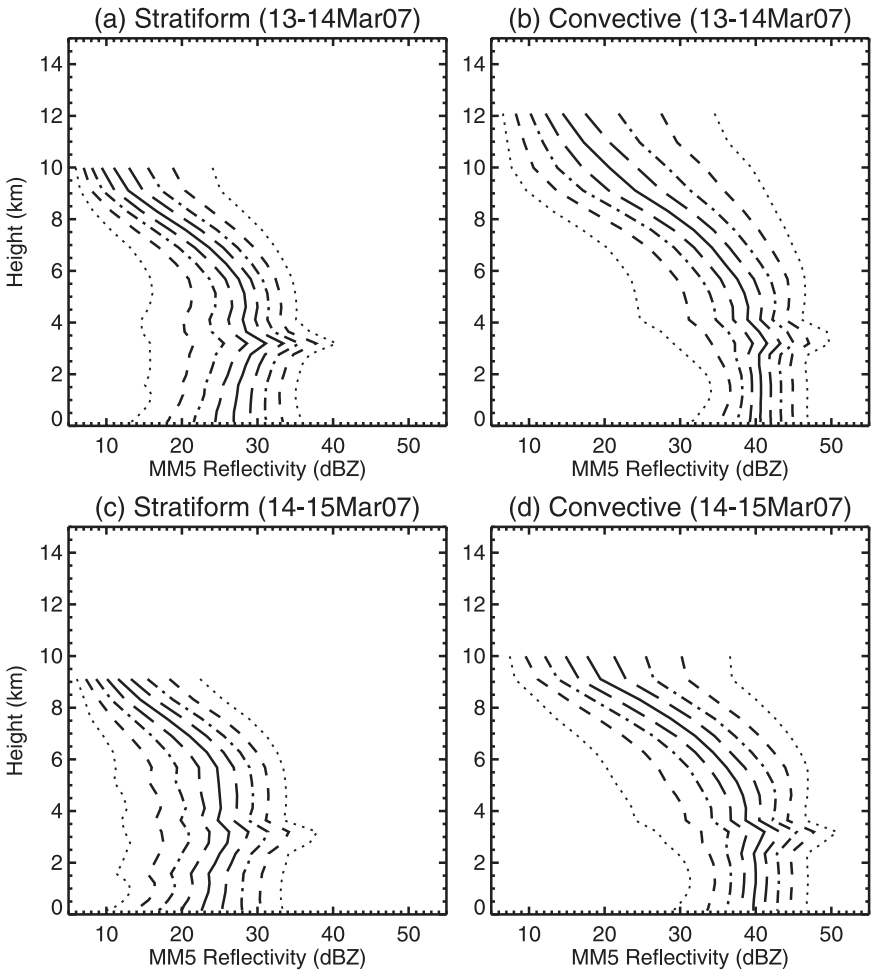

FIG. 9. Vertical distributions of radar reflectivity for stratiform and convective rain in MM5 (a),(b) from 1700 UTC 13 Mar to 1100 UTC 14 Mar 2007 and (c),(d) from 1400 UTC 14 Mar to 0400 UTC 15 Mar 2007.

larger below 8 km, and produce a stratiform region with stronger vertical velocities than occur in the barotropic case.

Finally, although convection on 14–15 March is largely forced by the low pressure system moving into the region, the 13–14 March storm may have had a small thermodynamic upscale feedback that assisted in enhancing convection the next day. Convection on 13–14 March is not as deep as in the barotropic case, but the storm's mean LND is only 0.4 km lower in MM5 and observations (Table 2), indicating that heating structures in some subtropical weakly baroclinic storms may be nearly as elevated as those in more barotropic environments. Convection does not form after the low pressure system passes in the wake of the 14–15 March storm, which has a lower stratiform area fraction and less elevated divergence profile. Mapes (1993) and Mapes and Houze (1995) have shown that stratiform rain in the tropics produces slow-moving gravity waves that heat the upper troposphere while cooling the lower troposphere, thus destabilizing the environment and encouraging convection to form. Circumstantially, some subtropical weakly baroclinic systems with deep convection and elevated heating profiles more characteristic of the tropics (like the 13–14 March storm) may also help drive additional convection as long as synoptic forcing mechanisms do not overwhelm diabatic convective feedbacks.

5. Model comparisons of additional upper-level disturbances

Three additional upper-level disturbances occurring in barotropic, weakly baroclinic, and strongly baroclinic environments (Table 1) have been simulated in MM5 to supplement the cases presented in the previous section.

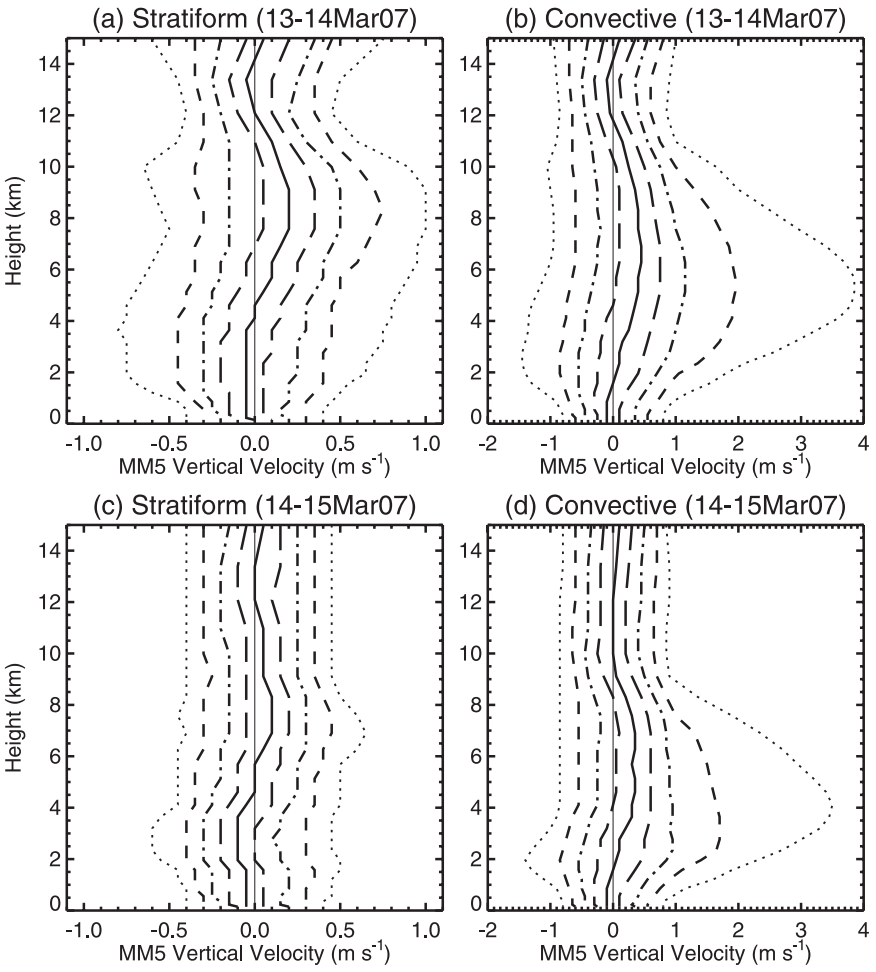

FIG. 10. Vertical distributions of vertical velocity for stratiform and convective rain in MM5 (a),(b) from 1700 UTC 13 Mar to 1100 UTC 14 Mar 2007 and (c),(d) from 1400 UTC 14 Mar to 0400 UTC 15 Mar 2007.

The barotropic upper-level disturbance consisted of airmass thunderstorms that rotated around a 500–700-hPa closed low pressure system located in central Texas on 4 July 2006. The model simulation accurately captures the organizational mode of convection rotating around the low with stratiform rain forming from aging convection, but is unable to pinpoint the exact timing and locations of individual cells (Figs. 11a,b). Area soundings also indicate that the environment was more tropical in nature with weak shear, deep moisture and precipitable water values above 60 mm. The initial mesoscale low pressure system originated on 30 June–1 July from a weak longwave trough, part of which cut off from the synoptic-scale flow and formed the upper-level low in question. Persistent convection over the next three days in the region may have helped maintain this low, which meandered around central Texas before beginning a slow eastward progression on 4 July and moving out of Texas on 6 July. Numerous airmass thunderstorms likely driven in part by diabatic convective feedbacks also formed on 5 July in southeast Texas near the propagating low.

This barotropic case is contrasted with two baroclinic upper-level disturbances whose synoptic forcing appears to overwhelm diabatic feedbacks. The weakly baroclinic upper-level disturbance formed in west Texas near Big Bend on 26 March 2007 in a trough cutoff from the main jet stream. As this midlevel trough became negatively tilted and the subtropical jet moved into the region from the southwest, the well-modeled storm matured into a large blobular MCS containing stratiform rain with regions of embedded convection (Figs. 11c,d). The storm slowly weakened and decreased in area early on 27 March before moving out of southeast Texas by 0900 UTC. The strongly baroclinic upper-level disturbance formed on 25 February 2006 in the left-exit region of a

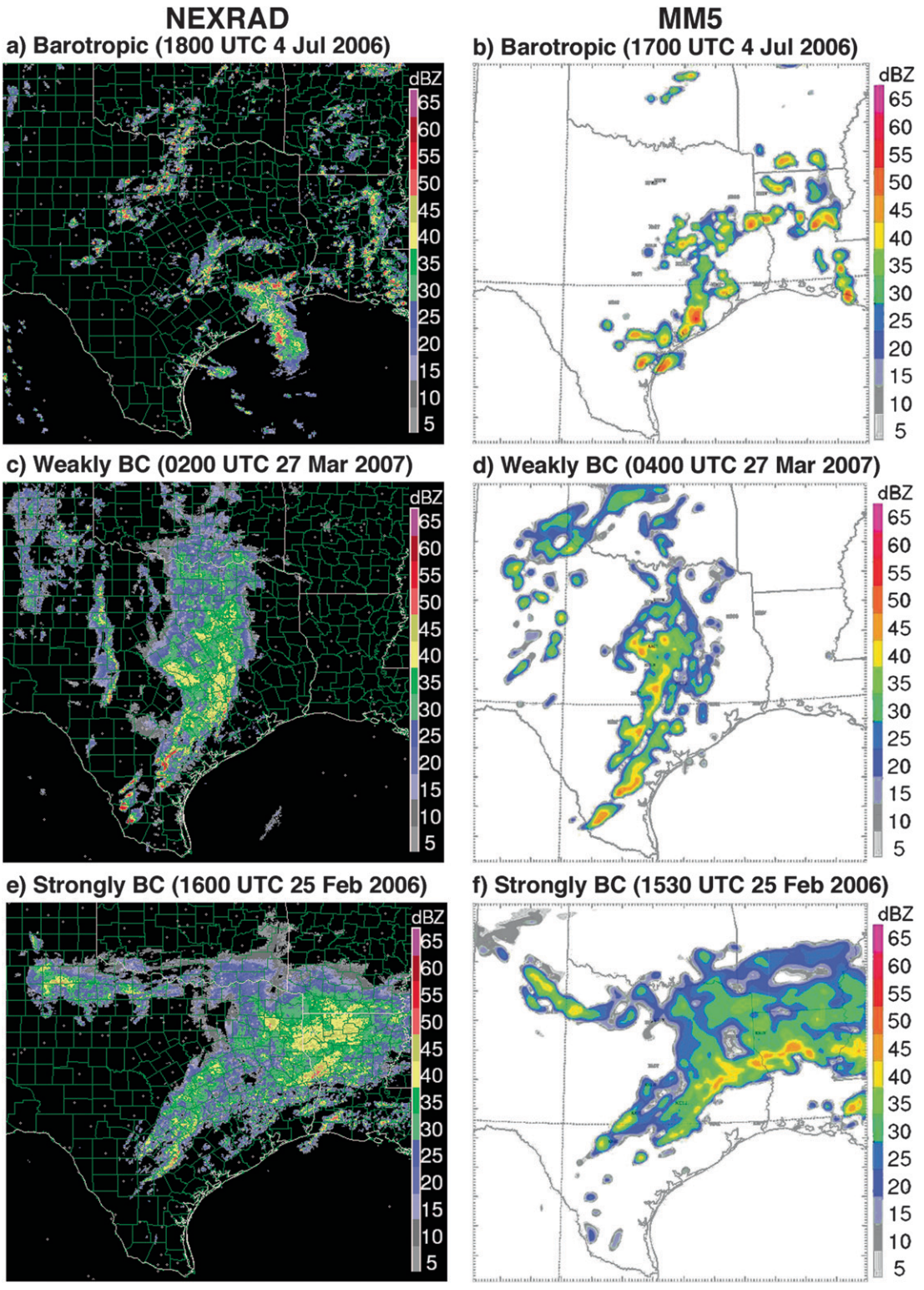

FIG. 11. (a),(c),(e) NEXRAD radar reflectivity and (b),(d),(f) MM5 reflectivity over D2 at the times indicated for each of the upper-level disturbance cases presented in section 5.

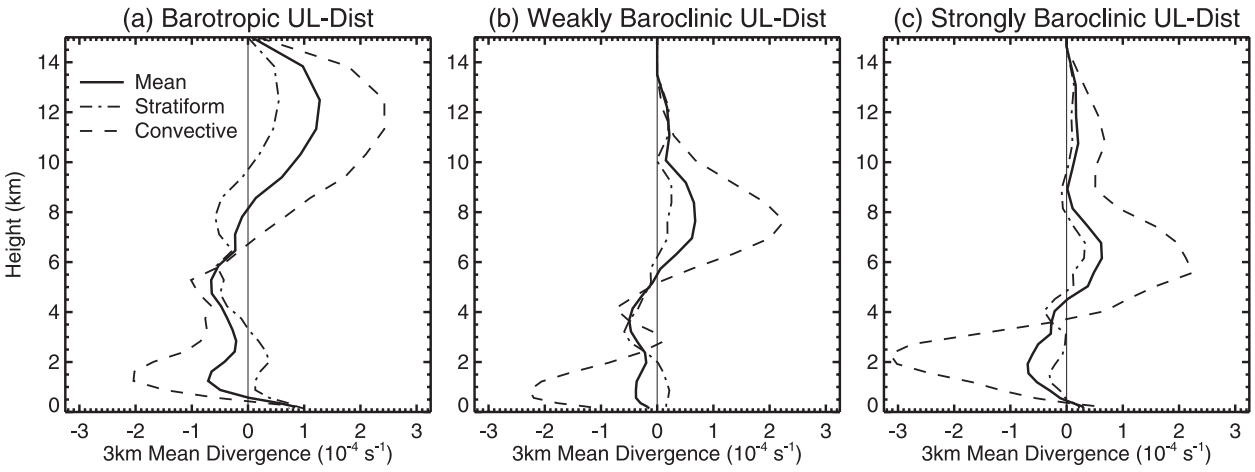

FIG. 12. MM5-derived mean grid-scale divergence profiles for the upper-level disturbance cases using half-hourly model data for stratiform (dash–dot) and convective (dashed) rain types as defined by the Steiner et al. (1995) separation algorithm applied to MM5-derived radar reflectivities. The profiles include all grid boxes in a vertical column for which the surface radar reflectivity exceeds 5 dB*Z*. (a) Barotropic mean divergence profiles from 1000 to 2300 UTC 4 Jul 2006. (b) Weakly baroclinic mean divergence profiles from 1900 UTC 26 to 1100 UTC 27 Mar 2007. (c) Strongly baroclinic mean divergence profiles from 0500 to 2200 UTC 25 Feb 2006.

subtropical jet downstream of a midlevel shortwave trough. This storm is also a well-modeled stratiform MCS (Figs. 11e,f), but with less embedded convection than the weakly baroclinic case. Area soundings indicate that temperatures were colder and that vertical wind shears were stronger for this storm than in the weakly baroclinic case, although the temperature gradient at the surface is still small. Even though a cold front was quickly moving in from Kansas and Oklahoma and a stationary front was situated in the Gulf, the precipitation formed between these far-removed frontal zones in response to the upper-level disturbances present and moved east during the afternoon.

Many of the divergence variations associated with increasing baroclinicity presented in section 4 are evident in the model-derived structures caused by these three storms. The barotropic case (Fig. 12a) generates the most elevated divergence profile with much higher mean, stratiform, and convective LNDs than the weakly baroclinic storm (Fig. 12b), which in turn has higher LNDs than the strongly baroclinic case (Fig. 12c; see also Table 2). Convective regions in both the barotropic and weakly baroclinic cases have a secondary peak in convergence near their melting levels of 5 km and 4 km, respectively, likely due to misclassification of some stratiform echoes. As a result, the convective profiles for these two storms have higher LNDs than they should, but this problem does not affect the mean (unseparated) divergence profile.

In agreement with the cases in section 4, mean upper-level divergence magnitudes are largest in the barotropic case, which has the greatest amount of deep convection, and decreases with increasing baroclinicity. However, the magnitudes of low-level convergence are smallest in the weakly baroclinic case and similar in the barotropic and strongly baroclinic cases, suggesting that these low-level variations are not necessarily attributable to baroclinicity and the amount of deep convection.

Stratiform area fractions (Table 2) are once again highest in the strongly baroclinic case (82.6%) and lowest in the barotropic case (61.3%) with the weakly baroclinic case falling in between (76.1%). Figure 12 shows distinct stratiform profiles with pronounced convergence at midlevels and divergence near the surface and at upper levels in the weakly baroclinic and barotropic cases, the latter of which has larger magnitudes and a thicker region of midlevel convergence because stratiform rain is arising from deeper, more tropical-like convection. Although stratiform rain results from relatively deep convection in the weakly baroclinic case as well, the tropopause is lower and prevents convection from penetrating as high into the atmosphere, which generates divergence profiles that are more compressed but similar in structure to the barotropic case. The strongly baroclinic stratiform divergence profile is much less pronounced, although it does exhibit a small convergent peak near the melting level at 4 km.

Although MM5 simulates higher LNDs for the 4 July 2006 storm (Fig. 12a) than on 20 July 2007 (Fig. 3a), both storms have similar stratiform area fractions (Table 2) and divergence structures. Their elevated mean divergence profiles coupled with a deep layer of midlevel convergence within stratiform rain suggest that

subtropical deep convection in some barotropic environments may behave like tropical deep convection (a result that is not just confined to one storm during the anomalous summer of 2007). In addition, extending the 4 July 2006 MM5 run for another 30 h (not shown) produces additional convection on D3 west of the low pressure system as observed on 5 July, implying that synoptic forcing mechanisms are not overwhelming diabatic convective feedbacks. Sensitivity tests suggest that incorporating the Grell cumulus parameterization scheme on D2 with 9-km grid spacing may simulate convection even better on 5 July than when convection is explicitly resolved. Although outside the scope of this study, additional research will need to determine the best model resolutions, parameterizations, and domain sizes to use for handling potential diabatic feedbacks in MM5 before comparing their effects on the global circulation in different subtropical and midlatitude regions.

6. Conclusions

MM5 simulations and ADRAD observations of precipitating systems associated with upper-level disturbances in southeast Texas contain mean divergence profiles whose magnitudes and structures vary across the region's wide spectrum of baroclinicities. Barotropic storms, which are common during the summer months, have the most elevated divergence structures (i.e., mean LNDs >6 km and maximum divergence above 11 km) because their tropopause heights are highest, allowing convection to penetrate higher and distribute mass flux perturbations over a greater depth of the atmosphere. Barotropic storms typically have the largest magnitudes of divergence because these storms tend to have the greatest amount of deep convection relative to stratiform rain (indicated by stratiform area fractions ~60%). As the degree of baroclinicity increases, stratiform area fractions generally increase and tropopause heights decrease, limiting the relative amount of convection and the height to which that convection can reach, respectively. However, some weakly baroclinic storms contain stratiform area fractions and divergence profiles with magnitudes and LNDs that are similar to barotropic storms, despite having lower tropopause heights and convection that is not as deep.

Robust stratiform and convective divergence signals were also obtained by applying Steiner et al.'s (1995) separation algorithm to MM5 reflectivity data, despite the fact that MM5 generates lower stratiform area fractions and higher radar reflectivities than typically observed. Barotropic storms have thicker and more elevated midlevel convergence in stratiform regions than in strongly baroclinic storms whose stratiform rain is caused by convection that penetrates through a much lower depth of the troposphere. Weakly baroclinic storms typically fall somewhere in between, depending on a particular storm's tropopause height and stratiform rain production mechanism (i.e., from deep convection or from large-scale lifting). Convective divergence profiles have more variable magnitudes and LNDs, although storms with lower degrees of baroclinicity have more elevated profiles associated with deeper convection (except for strongly baroclinic storms containing only elevated convection).

MM5's ability to generate reasonable convective and stratiform divergence profiles is encouraging because it implies that MM5 may adequately handle mass field perturbations in convective and stratiform regions, the latter of which are vital in producing diabatic feedbacks capable of driving additional convection as shown by Mapes (1993) and Mapes and Houze (1995). Elevated divergence profiles (particularly in stratiform regions) generated by storms like the 13–14 March 2007 case circumstantially suggest that heating at upper levels within stratiform regions may help drive additional convection in the subtropics and provides motivation to better quantify these potential diabatic feedbacks in the future.

Acknowledgments. Brian Mapes and Jialin Lin very kindly provided their CYLBIN code and analysis software for the ADRAD divergence calculations. Cameron Homeyer was instrumental in implementing the code and software at Texas A&M. We also thank Fuqing Zhang, Zhiyong (Ellie) Meng, and Jason Sippel for numerous helpful discussions about MM5 and Neil Smith and Shuguang Wang for the technical support they provided. Sandra Yuter, George Kiladis, Sharan Majumdar, and an anonymous reviewer also provided valuable advice and comments. This research is supported by NSF Grant ATM-0449782.

REFERENCES

Bell, G., and J. Janowiak, 1995: Atmospheric circulation associated with the Midwest floods of 1993. *Bull. Amer. Meteor. Soc.,* **76,** 681–695.

Blackadar, A. K., 1976: Modeling the nocturnal boundary layer. Preprints, *Third Symp. on Atmospheric Turbulence, Diffusion and Air Quality,* Raleigh, NC, Amer. Meteor. Soc., 46–49.

——, 1979: High resolution models of the planetary boundary layer. *Advances in Environmental Science and Engineering,* J. Pfafflin and E. Ziegler, Eds., Vol. 1, Gordon and Breach, 50–85.

Browning, K. A., and R. Wexler, 1968: The determination of kinematic properties of a wind field using Doppler radar. *J. Appl. Meteor.,* **7,** 105–113.

Cifelli, R., and S. A. Rutledge, 1998: Vertical motion, diabatic heating, and rainfall characteristics in north Australia convective systems. *Quart. J. Roy. Meteor. Soc.,* **124,** 1133–1162.

DeMaria, M., 1985: Linear response of a stratified tropical atmosphere to convective forcing. *J. Atmos. Sci.,* **42,** 1944–1959.

Dudhia, J., 1989: Numerical study of convection observed during the Winter Monsoon Experiment using a mesoscale two-dimensional model. *J. Atmos. Sci.,* **46,** 3077–3107.

——, 1993: A nonhydrostatic version of the Penn State–NCAR mesoscale model: Validation tests and simulation of an Atlantic cyclone and cold front. *Mon. Wea. Rev.,* **121,** 764–787.

Fritsch, J. M., and G. S. Forbes, 2001: Mesoscale convective systems. *Severe Convective Storms, Meteor. Monogr.,* No. 9, Amer. Meteor. Soc., 323–357.

Gamache, J. F., and R. A. Houze Jr., 1982: Mesoscale air motions associated with a tropical squall line. *Mon. Wea. Rev.,* **110,** 118–135.

Grell, G. A., 1993: Prognostic evolution of assumptions used by cumulus parameterizations. *Mon. Wea. Rev.,* **121,** 764–787.

Hartmann, D. L., H. H. Hendon, and R. A. Houze Jr., 1984: Some implications of the mesoscale circulations in tropical cloud clusters for large-scale dynamics and climate. *J. Atmos. Sci.,* **41,** 113–121.

Houze, R. A., Jr., 1982: Cloud clusters and large-scale vertical motions in the tropics. *J. Meteor. Soc. Japan,* **60,** 396–410.

——, 1993: *Cloud Dynamics*. Academic Press, 570 pp.

——, 1997: Stratiform precipitation in regions of convection: A meteorological paradox? *Bull. Amer. Meteor. Soc.,* **78,** 2179–2196.

Lang, S., W.-K. Tao, J. Simpson, and B. Ferrier, 2003: Modeling of convective–stratiform precipitation processes: Sensitivity to partitioning methods. *J. Appl. Meteor.,* **42,** 505–527.

Lin, Y.-L., R. D. Farley, and H. D. Orville, 1983: Bulk parameterization of the snow field in a cloud model. *J. Climate Appl. Meteor.,* **22,** 1065–1092.

Mapes, B. E., 1993: Gregarious tropical convection. *J. Atmos. Sci.,* **50,** 2026–2037.

——, and R. A. Houze Jr., 1993: An integrated view of the 1987 Australian monsoon and its mesoscale convective systems. Part II: Vertical structure. *Quart. J. Roy. Meteor. Soc.,* **119,** 733–754.

——, and ——, 1995: Diabatic divergence profiles in western Pacific mesoscale convective systems. *J. Atmos. Sci.,* **52,** 1807–1828.

——, and J. Lin, 2005: Doppler radar observations of mesoscale wind divergence in regions of tropical convection. *Mon. Wea. Rev.,* **133,** 1808–1824.

Reisner, J., R. M. Rasmussen, and R. T. Bruintjes, 1998: Explicit forecasting of supercooled liquid water in winter storms using the MM5 mesoscale model. *Quart. J. Roy. Meteor. Soc.,* **124,** 1071–1107.

Schumacher, C., and R. A. Houze Jr., 2003: Stratiform rain in the tropics as seen by the TRMM precipitation radar. *J. Climate,* **16,** 1739–1756.

——, and ——, 2006: Stratiform precipitation production over sub-Saharan Africa and the tropical East Atlantic as observed by TRMM. *Quart. J. Roy. Meteor. Soc.,* **132,** 2235–2255.

——, ——, and I. Kraucunas, 2004: The tropical dynamical response to latent heating estimates derived from the TRMM precipitation radar. *J. Atmos. Sci.,* **61,** 1341–1358.

Steiner, M., R. A. Houze Jr., and S. E. Yuter, 1995: Climatological characterization of three-dimensional storm structure from operational radar and rain gauge data. *J. Appl. Meteor.,* **34,** 1978–2007.

Stensrud, D. J., 1996: Effects of persistent, midlatitude mesoscale regions of convection on the large-scale environment during the warm season. *J. Atmos. Sci.,* **53,** 3503–3527.

——, and J. L. Anderson, 2001: Is midlatitude convection an active or passive player in producing global circulation patterns? *J. Climate,* **14,** 2222–2237.

Stoelinga, M., 2005: Simulated equivalent reflectivity factor as currently formulated in RIP: Description and possible improvements. White paper, 5 pp. [Available online at http://www.atmos.washington.edu/%7estoeling/RIP_sim_ref.pdf.]

Tao, W.-K., and J. Simpson, 1993: Goddard cumulus ensemble model. Part I: Model description. *Terr. Atmos. Oceanic Sci.,* **4,** 25–72.

Wallace, J. M., and P. V. Hobbs, 1977: *Atmospheric Science, An Introductory Survey*. Academic Press, 467 pp.

Yuter, S. E., and R. A. Houze Jr., 1997: Measurements of raindrop size distributions over the Pacific warm pool and implications for Z–R relations. *J. Appl. Meteor.,* **36,** 847–867.

Zhang, D.-L., and R. A. Anthes, 1982: A high-resolution model of the planetary boundary layer—Sensitivity tests and comparisons with SESAME-79 data. *J. Appl. Meteor.,* **21,** 1594–1609.

——, and J. M. Fritsch, 1986: Numerical simulation of the meso-β scale structure and evolution of the 1977 Johnstown flood. Part I: Model description and verification. *J. Atmos. Sci.,* **43,** 1913–1943.